Carlos López, Ángel F. Doval, Benito V. Dorrío, Daniel Cernadas, Cristina Trillo, José L. Fernández, Mariano Pérez-Amor and Benjamín G. Tejedor, "Spatial resolution and MTF of a fibreoptic probe for the automatic inspection and measurement of surface cracks in the inner side of heat exchanger tubes," Proc. SPIE 4185, "14th International Conference on Optical Fiber Sensors", 218-221 (October 2000)

Copyright 2000 Society of Photo-Optical Instrumentation Engineers.
This paper was published in "Proceedings of SPIE" and is made available as an electronic reprint with permission of SPIE. One print or electronic copy may be made for personal use only. Systematic or multiple reproduction, distribution to multiple locations via electronic or other means, duplication of any material in this paper for a fee or for commercial purposes, or modification of the content of the paper are prohibited.

http://dx.doi.org/10.1117/12.2302214

Spatial Resolution and MTF of a Fibreoptic Probe for the Automatic Inspection and Measurement of Surface Cracks in the Inner Side of Heat Exchanger Tubes

C.López , A. F. Doval, B. V. Dorrío, D. Cernadas, C. Trillo, J.L. Fernández, M. Pérez-Amor, B. G. Tejedor†

Universidade de Vigo, Dpto. Física Aplicada, Lagoas-Marcosende, nº9, 36200 VIGO, Tf. (34) 986 812216, 812194, FAX (34) 986 812201

†TECNATOM,S.A., Avda. Montes de Oca, nº 1, 28709 San Sebastián de los Reyes, MADRID Tf. (34) 916 598600, FAX (34) 916 598677

ABSTRACT

The resolution performance of a new fiberoptic probe is analysed using its MTF and its resolution limit that are evaluated both with a simple theoretical model and with experimental data obtained with a laboratory prototype.

1. INTRODUCTION

The inspection of heat exchanger tubes by eddy currents techniques is established and present high performance, but the measurement principle imposes limitations both to the achievable resolution (~1 mm) and also, in tubes with supporting plates, for inspecting the tubes at the neighbourhood of the plates[1]. Among several trails in the last decade to overcome these problems using optical principles[2,3] we have proposed[4] a new technique based on a fibreoptic probe that obtains an image of the surface using small fibre reflectometers that cover simultaneously a ring section of the tube (fig. 1). The image brightness assigned to each point Q is proportional to the average value of the irradiance E_F over the detection fibre input face. If the 1D circumferential scanning is combined with a 1D axial scanning, a global image is obtained in which cracks will appear as dark areas.

Part of a detailed analysis of this technique[5] has been already published[6]. The analysis includes, by one hand, a specifically developed theoretical model that describes the imaging process of the probe as a linear system (fig. 2a). The main hypothesis of the model is that the intensity is spread by the normal areas of the surface inside a cone of semiangle θ_D and, at a distance QB from the surface, the length of the spread is given by

$$M = 2 \cdot QB \cdot \tan\theta_D \tag{1}$$

In the simplest case of sampling pitches p_c and p_a lower enough to consider the output as a continuous function, for a infinite straight crack of width δ oriented along the circumferential or axial direction (y direction in fig. 2c) the imaging process can characterised by a line spread function $l_{DF}(x_F)$ that relates the output irradiance $e_F(x)$ and the surface reflectance $r(x)$ (fig. 2b1, and table 1: Row 3-Colum 1 (T1: R3-C1)). $l_{DF}(x_F)$ can be used to predict the output profile of a crack and to establish the basic relation

$$\delta_F = \delta + M + D \tag{2}$$

from which δ can be measured using δ_F, provided that M and D are known (fig. 2c).

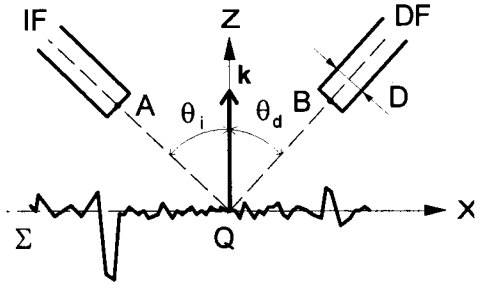

Fig. 1: Scheme of the reflectometric configuration: IF: illumination fibre, DF: detection fibre, Σ: surface, θ_i: mean angle of illumination, θ_d: mean angle of detection, **k**: normal to the surface mean level, QB: detection distance, D: size of the input face of the detection fibre. The detection fibres are disposed with rotational symmetry around the axis of the tube and the points Q (defined as the intersection of each detection fibre axis with the surface mean level) are equally spaced along the circumferential direction with pitch p_c equal to the circumference length divided by the number of detection fibres.

By the other hand, the experimental analysis have shown[8] that the theory is well correlated with the behaviour of isolated cracks over the inner surface of heat exchanger tubes of Inconel 800 characterised by a spread $\theta_D \cong 5^0$. In the present work, we briefly present the theoretical model in the frequency domain and obtain the theoretical values of MTF and spatial resolution limit that will be compared with the experimental data.

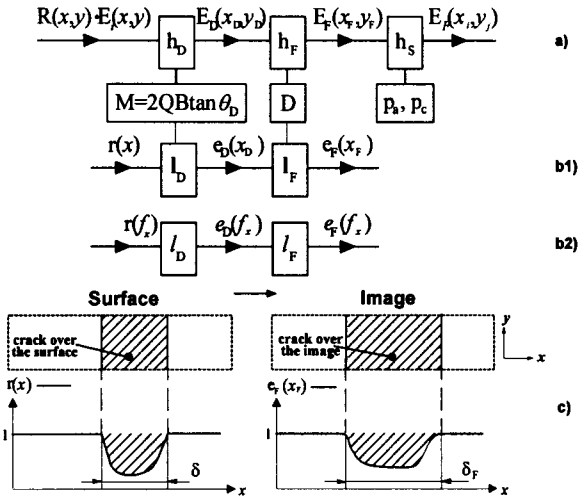

Fig. 2:a) Scheme of the image formation process as a linear system: $R(x,y)$ surface reflectance, $E_i(x,y)$ incident irradiance, $E_D(x,y)$ irradiance at the detection plane, $E_F(x,y)$ integrated irradiance by the fibre, $E_F(x_F,y_j)$ sampled values of $E_F(x,y)$, h_D impulse response related to the effect of the diffusive behaviour of the surface and characterised by the parameter M, h_F impulse response related to the integration by the detection fibres and characterised by the size of the fibre input face D, h_S not shift-invariant impulse response related to the sampling process and characterised by the sampling pitches p_c and p_a

b1) Scheme of the image formation process for a straight crack of width δ, $r(x)$, $e_D(x)$ and $e_F(x)$ normalised values of R, E_D and E_F, l_D and l_F line-spreads corresponding to the point-spreads h_D and h_F. b2) The same that in b1) in the frequency domain. c) Relationship between the normalised reflectance distribution $r(x)$ of the surface and the output integrated irradiance $e_F(x)$ in the image and between the widths of the crack over the surface δ and over the image δ_F.

2. THEORY: MTF AND RESOLUTION LIMIT

The expression for the image forming process in the spatial frequency domain (T1: R3-C2) relates the input and output Fourier spectrum $r(f_x)$ and $e_F(f_x)$ by means of the Optical Transfer Function $l_{DF}(f_x)$ (T1: R1-C2). For each MTF (T1, R1-C3) we can define the corresponding resolution limit as $r=1/f_c$, where f_c is the minimum spatial frequency for which the selected MTF goes to zero. Taking into account that for a given type of surface (θ_D=constant) M is reduced only reducing QB, we conclude that, if QB is kept constant, the best value of r_{DF} is given by M provided that D≤M (T1: R1-C4 and fig. 3).

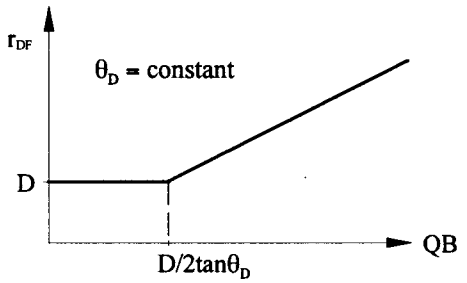

Fig. 3 Evolution of the theoretical value of the resolution limit r_{DF} as a function of the detection distance QB for a constant value of the diffusive behaviour of the surface θ_D and the fibre size D.

As $M_{DF}(f_x)$ and r_{DF} (T1: R1-C3,4) depend on M, to check the validity of the theory we have had to design a not-standard approach for MTF evaluation based on reference patterns of cracks performed over the previously tested tubes[6] (in this case $\theta_D \cong 5^0$). The basic hypothesis of our scheme is that the reflectance of a pattern $r_P(x)$ of length L can be described as a finite train of pulses (T1:R4,5-C1). When L is much greater than the pitch of the pattern (i.e. $L \cong q\Lambda >> \Lambda$, q integer) the spectrum of $r_P(x)$ at frequencies n/Λ can be evaluated as a function of the spectrum for an infinite train $r(x)$ (T1: R4,5-C2) and so we can obtain the expressions[5]

$$M_{DF}(n/\Lambda) = \left\| \frac{e_F(n/\Lambda)}{e_F(0)} \right\| \cdot \left| \frac{r_P(0)}{r_P(n/\Lambda)} \right| = \left\| \frac{e_F(n/\Lambda)}{e_F(0)} \right\| \cdot \left| \frac{n\pi\{1-\{1-r_M\}\delta/\Lambda\}}{\{1-r_M\}\,\mathrm{sen}(n\pi\delta/\Lambda)} \right| \quad (3)$$

$$r_M = 1-(\delta/\Lambda)(1-e_F(0)/L) = 1-(\delta/\Lambda)(1-[e_F(x_F)]) \quad (4)$$

On the basis of (3) and (4) and the values Λ and δ of the reference crack pattern, the MTF can be evaluated at n/Λ (n=0,1,2,...) using the Fourier Transform values $e_F(n/\Lambda)$ that can be extracted from the experimental data.

3. EXPERIMENT

The experiments were performed over tubes of diameter 16.8 mm diametrically sectioned (equal to real steam generator tubes) with regular patterns created by electrical disintegration. The patterns have straight cracks with different widths δ and with pitches Λ 100 and 250 μm. A set of images of the patterns was taken with a laboratory prototype[5,6] that allows to select independently the parameters of the reflectometric configuration and the sampling pitches. All the images were obtained using the same values of the illumination and detection angles (θ_i=θ_d=30°) and selecting p_x=1 to minimise the effect of sampling along the x direction

	C1		C2		C3		C4
	Line Spread Function $g(x)$		One-dimensional OTF $g(f_x)=\int_{-\infty}^{\infty} g(x)\cdot\exp(-j2\pi x f_x)\cdot dx$		One-dimensional MTF $MTF=\|g(f_x)\|$		Resolution
	Name	Expression	Name	Expression	Name	Expression	Limit
R1	$l_D(x_D)$	$\frac{1}{M}\cdot rect\left\{\frac{x_D}{M}\right\}^*$	$l_D(f_x)$	$\frac{sen\{\pi M f_x\}}{\pi M f_x}$	$M_D(f_x)$	$\left\|\frac{sen\{\pi M f_x\}}{\pi M f_x}\right\|$	$r_D = M$
	$l_F(x_F)$	$\frac{1}{D}\cdot rect\left\{\frac{x_F}{D}\right\}$	$l_F(f_x)$	$\frac{sen\{\pi D f_x\}}{\pi D f_x}$	$M_F(f_x)$	$\left\|\frac{sen\{\pi D f_x\}}{\pi D f_x}\right\|$	$r_F = D$
	$l_{DF}(x_F)$	$\int_{-\infty}^{\infty} l_F(x_F-x_o)\cdot l_D(x_o)\cdot dx_o$	$l_{DF}(f_x)$	$\frac{sen\{\pi M f_x\}}{\pi M f_x}\frac{sen\{\pi D f_x\}}{\pi D f_x}$	$M_{DF}(f_x)$	$\left\|\frac{sen\{\pi M f_x\}}{\pi M f_x}\frac{sen\{\pi D f_x\}}{\pi D f_x}\right\|$	$r_{DF} = max\{M,D\}$
R2	$l_G(x_F)$	$\sqrt{\frac{2}{\pi}}\cdot\frac{1}{M+D}\cdot\exp\left\{-2\left\{\frac{x}{M+D}\right\}^2\right\}$	$l_G(f_x)$	$\exp\left\{-\frac{1}{2}\{\pi(M+D)f_x\}^2\right\}$	$M_G(f_x)$	$\exp\left\{-\frac{1}{2}\{\pi(M+D)f_x\}^2\right\}$	$r_G \cong M+D$ ‡
	Spatial domain		Fourier domain				
R3	$e_F(x_F)$	$\int_{-\infty}^{\infty} l_{DF}(x_F-x)\cdot r(x)\cdot dx$	$e_F(f_x)$	$l_{DF}(f_x)\cdot r(f_x)$			
R4	$r(x)$	$1-(1-r_M)\sum_{n=-\infty}^{+\infty} rect\left\{\frac{x-n\Lambda}{\delta}\right\}$	$r(f_x)$	$f_x=0:\left\{1-(1-r_M)\frac{\delta}{\Lambda}\right\}$			
				$f_x\neq 0:(1-r_M)\frac{sin\{n\pi\delta/\Lambda\}}{-n\pi}\bar{\delta}\left\{f_x-\frac{n}{\Lambda}\right\}$ †			
R5	$r_P(x)$	$r(x)\cdot rect\left\{\frac{x}{L}\right\}$	$r_P(f_x)$	$f_x=0:L\left\{1-(1-r_M)\frac{\delta}{\Lambda}\right\}$			
				$f_x=n/\Lambda:\frac{\{1-r_M\}\cdot L}{-n\pi}sin\left(\frac{n\pi\delta}{\Lambda}\right)$			

Table 1: R1) Line-spread, OTF and MTF of the imaging process; R2) Gaussian line-spread, OTF and MTF; R3, R4 and R5) Expression for the imaging process and the reflectance of an infinite and a finite train of cracks respectively. *rect(x) is a square pulse of width 1 and height 1. ‡ In this case the cut-off can be defined as a function of the standard deviation. † $\bar{\delta}\{f_x\}$ Dirac Delta Function

The raw images were processed with an automatic algorithm that extracts a reduced data set (fig. 4). The analysis is developed in J=9 parallels profiles of each image. Using the mean level of each profile the points are classified in normal areas N or pattern areas P. With the mean values of each class E_{FPj} and E_{FOj}, the mean value of the pattern profile results $[e_F(x)]=E_{FPj}/E_{FOj}$ that with (4) gives r_{Mj}. Then, the profile of the class P is normalised to $e_{Fj}(x_i)$ using E_{FPj} and truncated to a length L with a number of points multiple of 2. Using a standard FFT algorithm we find the discrete one-dimensional Fourier transform $e_{Fj}(k/L)$ (fig. 5). r_{Mj} and the modulus of $e_{Fj}(n/\Lambda)$ are averaged over j to obtain the reduced data $[r_M]$ and $[e_F](n/\Lambda)]$ that with (3) give the experimental value of the MTF $[M_{DF}(n/\Lambda)]$.

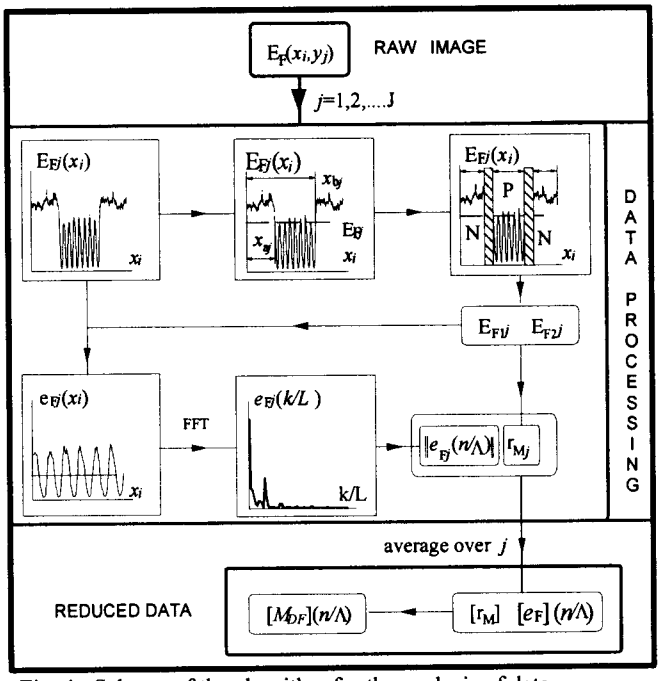

Fig. 4 Scheme of the algorithm for the analysis of data.

The results shown that $[M_{DF}(n/\Lambda)]$ is, for any combination of QB and D and n, lower than the theoretical value $M_{DF}(f_x)$ (fig. 6). But, as the cut-off frequency is close to the theoretical value (fig. 6b), the model can predict with reasonable accuracy the resolution limit (if D≤M, $r_{DF} \cong 40$ μm with QB≅200 μm). On this basis, and taking into account that a) the agreement between theory and experiment in the case of isolated cracks is based mainly in the value of the maximum widths M and D of the spreads $l_D(x)$ and $l_F(x)$ and not in their particular expressions (T1: R1-C1) and b) that the data can be fitted to a gaussian MTF $M_G(f_x)$ (fig. 6) (i.e. for a gaussian linear spread $l_G(x)$) defined as a function of model parameters M and D (T1-R2), we can conclude that M and D are adequate parameters to

describe the spreads in the image formation process, but the detailed value of the line spread has to be revised.

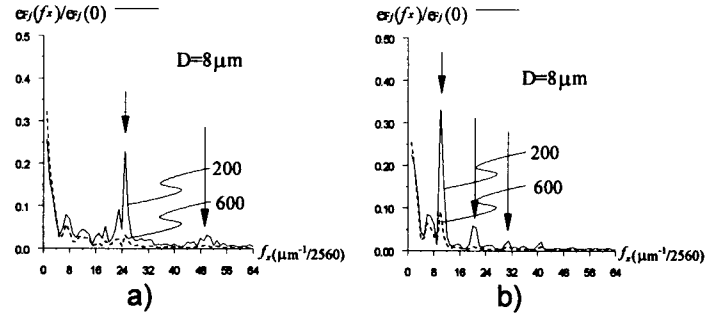

Fig. 5: Zoom of the One-dimensional Discrete Fourier Transforms (DFT) of the integrated irradiance for a profile of a crack pattern from images obtained using D=8 μm with two values of QB (QB is in microns in the figure). The arrows locate the positions of the harmonics (n=1 is the fundamental spatial frequency): a) δ= 70 μm and Λ= 100 μm. b) δ= 125 μm and Λ= 250 μm.

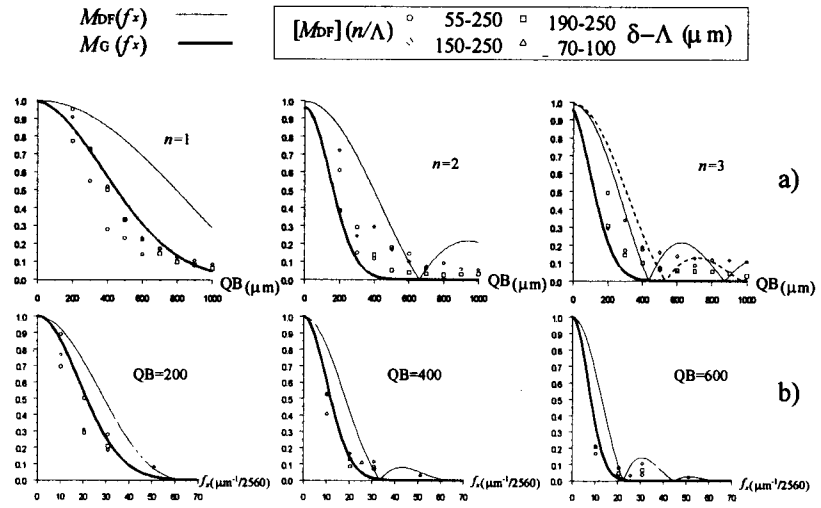

Fig. 6: a) Evolution with QB of the values of the MTFs $M_{DF}(f_x)$ (theory) and $[M_{DF}](f_x)$ (experiment) for different harmonics (n=1, 2, 3) from images obtained with D=8 μm. b) Comparison between the values of the MTFs $M_{DF}(f_x)$ (theory) and $[M_{DF}](n/\Lambda_x)$ (experiment) from images obtained with D=40 μm and different values of QB (QB is in microns in the figure). The value of the gaussian MTF $M_G(f_x)$ (theory) is also plotted

4. CONCLUSION

The resolution performance of a new fiberoptic probe for automatic detection and measurement of cracks has been analysed. The comparison between theory and experiment show that, even though the theoretical model and the parameters M and D are adequate to describe both isolated cracks and the resolution limit, a better matching between theory and experiment should be attained if a suited line spread function is selected. A line-spread of gaussian form could be a solution to this problem.

5. ACKNOWLEDGEMENTS

The authors acknowledge the financial support of UNESA (Group of Spanish Electrical Utilities) and TECNATOM, S.A during the development of this research work.

6. REFERENCES

1. P. Cielo, Optical Techniques for Industrial Inspection, 1st ed. (Academic Press, San Diego, 1988), Chap. 1.
2. Electric Power Research Institute, projects S103-1 & S103-2, "Optical scanner system for the internal inspection of steam generator tubes", sponsored by the "Steam Generator Owners Group", USA, (1980-81).
3. J.L. Doyle, "Applications of laser-based surface profilometry to tubing in power generation utilities", Proc. SPIE, Vol.2454, pp.91-103, (1995).
4. C. López, A.F. Doval, B.V. Dorrío, R.Soto, J. Blanco-García, J.L. Fernández, M.Pérez-Amor, B.G. Tejedor, "New fibreoptic laser probe for the automatic inspection of cracks in the inner side of heat exchanger tubes of nuclear power plants", Proc. SPIE **2247**, pp. 4-14, (1994).
5. C. López, "Nuevas técnicas ópticas para la inspección y medida automática de defectos en tubos de intercambiadores de calor", PhD. Thesis, Uni. de Vigo, (1997).
6. C. López, A.F. Doval, B.V. Dorrío, . Blanco-García, J. Bugarín, J.M. Alén, A.Fernández, J.L. Fernández, M.Pérez-Amor, B.G. Tejedor, "Fibreoptic reflectometric technique for the automatic detection and measurement of surface cracks", Meas. Sci. Technol., 9, pp. 1413-1431, (1998)